SCOPE | SAUDI INTERNATIONAL CONFERENCE ON NUCLEAR POWER ENGINEERING

Proceedings of SCOPE
13-15 Nov. 2023 – KFUPM
Paper 23084

In-Core Power Mapping for an HPR1000 using an Indigenous Program for Depletion Calculation & Machine Learning

Ibrahim Patel*, Rizwan Ahmed, Syed Nadeem Ahsan, Syed Uzair Ahmed, and Muhammad Usman Naseem
Karachi Institute of Power Engineering (College of Pakistan Institute of Engineering & Applied Sciences)
Karachi, Pakistan
**Corresponding author email: ipatel.me@gmail.com*

Abstract – *The application of Artificial Intelligence (AI) is widespread in several fields, including nuclear power engineering. A nuclear reactor can be safely and optimally operated when various safety metrics, such as the power peaking factor and the departure from nucleate boiling ratio, are reliably obtained from the core power distribution. The failure of in-core instrumentation poses a challenge to continued safe and reliable operation, and risks in forced shut down to ensure core integrity. This work sought to apply suitable Machine Learning techniques for In-Core Power Mapping of a Hualong One (HPR1000), based upon reactor core simulations of the first fuel cycle; using an indigenously developed program for depletion calculation, and available operational data. Beginning with the reactor core simulations and intuitive choice of parameters for power density prediction, different Regression techniques have been explored. For full power map reconstruction, using the power density values available at detector locations, Two-Layer Feed-Forward (TLFFNs) and Convolutional Autoencoder Networks (CANs) have been explored. Utilizing actual detector charge data, Long Short-Term Memory Networks (LSTMNs) have been trained for temporal prediction of charge for multiple detector failures. Using actual data for charge and relative power distribution, LSTMNs and TLFFNs, used in conjunction, have been found suitable for extending plant operation for a few hours for up to 50% of detector failures. Prediction of temperatures based on power prediction is also proposed and demonstrated to validate against measured temperatures for practical implementation. Graphical User Interfaces (GUIs), implementing the best of explored techniques, have also been developed for In-Core Power Mapping.*

Keywords: Power Mapping, Artificial Intelligence, Machine Learning, Deep Learning, Hualong One, Pressurized Water Reactor

I. Introduction

The research and applications of Artificial Intelligence (AI) are being pursued in several technical fields, including nuclear power engineering. The long-term consideration for several aspects of the application of AI in the nuclear industry has been published by the International Atomic Energy Agency (IAEA) and the United States Nuclear Regulatory Commission (USNRC) with a welcoming attitude for solutions leveraging AI **[1-2]**.

Continuous core operation condition monitoring, using power and temperature distributions, is essential to ensure that the reactor runs efficiently and safely. To monitor the changes in power distribution, neutron flux is measured at various core locations, using neutron detectors, such as Self-Powered Neutron Detectors (SPNDs). Similarly, the temperature distribution is measured using temperature sensors, such as thermocouples.

Thermal limits, such as the minimum departure from nucleate boiling ratio (DNBR), linear power density, and anomalies, such as hot spots, dropped and misaligned rods, fuel misloading and xenon oscillations

may be detected from the reconstructed in-core power distribution in online Core Monitoring Systems (CMS) **[3-4]**.

The application of Artificial Intelligence (AI) for power distribution and safety metrics determination, has been done by several authors **[3,5-6]**. This project has been undertaken to indigenize core power mapping using an indigenous program for depletion calculation (PFDC), coupled with machine learning (ML) techniques for the two units of Hualong One (HPR1000) commissioned in Pakistan **[7]**.

The failure of SPNDs causes a loss of information about the neutron flux, and consequently, the power distribution in the core, which puts reactor operation at risk. Partial failure can cause erroneous readings and false perceptions of the actual core condition that may lead to incorrect decisions **[8]**. A method is needed to reliably determine the core power distribution for the safe, smooth, and efficient operation of any Nuclear Power Plant (NPP), despite instrumentation failure. Otherwise, the plant has to be shut down, as per regulatory requirements, when more than 25% of in-core detectors fail, failing to meet a Limiting Condition for Operation (LCO) **[9]**.

II. Background

II.A. Machine Learning

Machine Learning (ML) is distinct from programming, wherein a computer develops models based on data. ML encompasses two major techniques: *supervised learning*, where models are trained on known predictor(s) and target data, and *unsupervised learning*, which discovers patterns in input data. Supervised learning includes *classification* (to predict discrete responses) and *regression* (to predict continuous variables) **[10]**.

Deep Learning is a subset of ML that is inspired by the human brain's complex neural network. *Feedforward networks* consist of multiple layers. The first layer acts as the network's input, with each succeeding layer linked to the preceding one. The output of the network is produced by the last layer. A feedforward network with a single hidden layer and enough neurons has the potential to solve any finite input-output mapping problem **[11-12]**.

Convolutional Autoencoder Networks (CANs) are employed for image denoising, using an encoding and decoding stage.

A *Long Short-Term Memory Network* (LSTMN) is used for data sequence prediction. There are two methods of forecasting using LSTMNs: open-loop and closed-loop.

Open-loop forecasting predicts future time steps in a sequence using real-time data input. Whereas closed-loop forecasting predicts using the LSTMN's former prediction as input. Closed-loop forecasting can be used to predict when real-time data is not available to the network before making the next prediction **[12]**.

II.B. Machine Learning Performance Metrics

Many metrics can be used to assess ML performance. The most basic is the residual, r_i, which is the difference between the true value, y_i, and the model's predicted value, $\hat{y}_i$. Where i denotes the sample index from n samples, that is $i = 1,2,\dots n$. All other metrics are summary statistics for the residual.

Relative to the true value of the response, r_i yields the relative error, whose average over all samples can be reported as a percentage, called the Mean Absolute Percentage Error (MAPE).

Mean Square Error (MSE) is the average sum of squared residuals. MSE is sensitive to large errors and outliers. The Root Mean Square Error (RMSE) is the square root of the MSE, that has the same unit as the response variable.

The performance of Convolution Networks can be assessed using image quality metrics, comparing the output image relative to its true or ideal image. The structural similarity (SSIM) index combines various image properties into a single local quality score. It is like quantifying human visual perception **[12]**.

II.C. Machine Learning for Core Monitoring Systems

Continuous monitoring of reactor parameters is essential during plant operation to ensure safe and efficient performance. Core Monitoring Systems (CMS) process raw data from in-core instrumentation to generate key outputs including; assembly and pin-wise power distribution, thermal-hydraulic characteristics (such as DNBR), and indicators for detection of deviation from normal operation **[13]**.

Recent research has explored supplementing CMS with operational data-driven models using ML. Li et al. investigated the reconstruction of the core power distribution for a Pressurized Water Reactor (PWR) using combinations of in-core, ex-core, and thermocouple detectors **[3]**. They found that Multi-Layer Perceptron networks provided robust reconstruction compared to more sensor-sensitive Radial Basis Function networks. The authors suggested

that convolution neural networks (CNN) may further improve accuracy by incorporating spatial layout information.

Saeed and Rashid combined an ANN model with the reactor physics code, INCOPW, to estimate Power Peaking Factors (PPFs) and safety metrics for a PWR **[5]**. Online validation during the 11th fuel cycle showed that their modified CMS could enable core monitoring for similar NPPs at the station.

Pirouzmand and Dehdashti used ANNs to forecast power distributions and PPFs across 200 states of a VVER-1000 reactor **[6]**. Their model fits well with the validation data (with less than 3% error). They found the radial power distribution most sensitive to control rod positions and ex-core neutron detector signals.

III. Core Simulation and Machine Learning

Hualong One has been simulated using an indigenous program for depletion calculation (PFDC) to generate datasets for predicting and reconstructing the core power density distribution using ML. Available plant operational data has been used for core power mapping with temporal predictions during multiple SPND failures. A simple calculation scheme to estimate the core exit temperature, based on predicted power, is also proposed as a validation scheme for the temporal predictions. Fig. 1 illustrates the overall flow of data for this work.

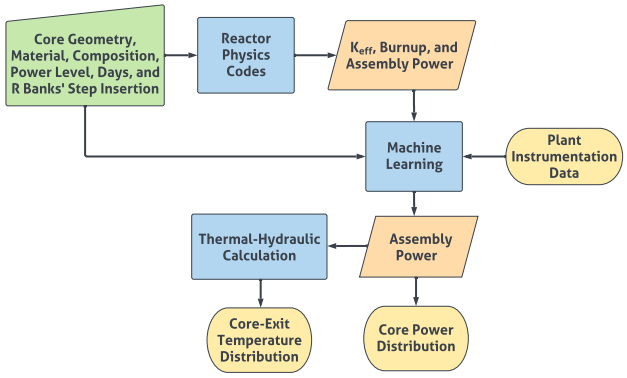

Fig. 1. Work Scheme for Core Power Mapping.

III.A. Hualong One

The Hualong One (HPR1000) is a Generation III+ NPP (PWR type), created by the China National Nuclear Corporation (CNNC), incorporating several active and passive safety features. The HPR1000 is designed to generate 1090 MWe from 3050 MWt, with three coolant loops. The core is composed of 177 fuel assemblies that use SPNDs to measure neutron flux and reconstruct full core power distribution. 7 SPNDs are axially distributed at 44 symmetric radial positions **[14]**.

III.B. Program for Depletion Calculation, Simulation Data Generation, and Processing

An indigenous algorithm for the combined use of WIMS and CITATION, named *Program for Depletion Calculation* (PFDC) has been used for simulating HPR1000 neutronics. After defining the geometry, material, and burnup calculation steps for the computational cells, WIMS calculates the assembly averaged nuclear cross-sections that CITATION uses for iteratively calculating k_{eff}, power, and burnup for the given core geometry until k_{eff} is unity, corresponding to the reactor's critical condition. Fig. 2 illustrates the PFDC algorithm.

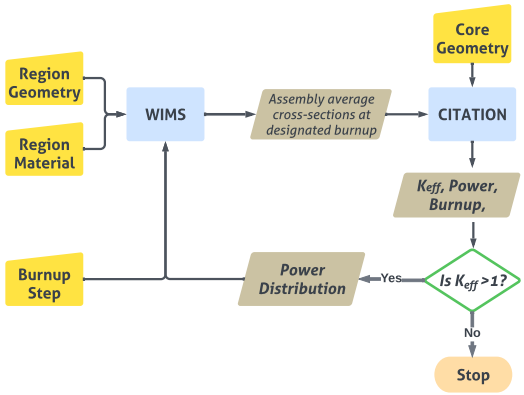

Fig. 2. Algorithm for HPR1000 simulation.

The model uses 1/8th core symmetry for burnup computations of 29 assemblies. There are 31 computational regions to incorporate the effect of assemblies with 'R' control banks.

Two arbitrary load schedules were devised to simulate the core for 336 Effective Full Power Days. The load schedules varied between 50 and 100 % full power with arbitrary duration, and appropriate calculation steps to obtain the inter-transitory trend of the calculated parameters.

The data was compiled in a spreadsheet, having 4,814 data points for: the operational time elapsed, axially averaged assembly-wise power density, fuel burnup, core power level, R-bank limit insertion ($\mathcal{R}$), and the effective multiplication factor (k_{eff}). The assembly enrichment, number (1-29), and x - y coordinates were included as identifiers/tags for each fuel assembly.

III.C. Regression

For regression, power density was used as the target variable, with others as the predictor variables. 75% of the dataset was used for training with 10-fold cross-validation, and 25% of the dataset was reserved as test data to check the accuracy of trained models.

Based on *Fine Tree Regression* (because of the brief time it requires training), the predictor variables were reduced by assessing the sensitivity of the RMSE on the test data with different combination of predictors.

III.D. Two-Layer Feed-Forward Network

1) Simulation Data

10 identical two-layer feed-forward neural networks (TLFFNs) were trained with simulation data from one of the two load schedules, with randomly initialized weights (w) and biases (b), for selecting the network with the lowest error score on a common test dataset.

The input dataset consisted of 44 input values of power density (assemblies with SPNDs), and the output consisted of 133 values of power density (assemblies without SPNDs). The training dataset spanned 85 simulated days. The input and output datasets were represented as arrays of numeric values, 44x85 and 133x85, respectively.

The TLFFN architecture consisted of a hidden layer, with 10 sigmoid hidden neurons, and the tan-sigmoid activation function. The output layer consisted of 133 linear output neurons. Fig. 3 illustrates the architecture of the TLFFN.

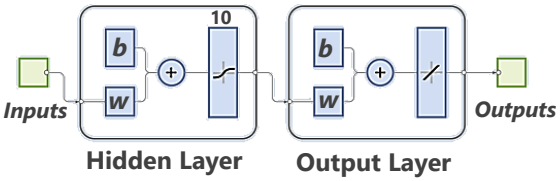

Fig. 3. Two-Layer Feed-Forward Network Architecture.

2) Plant Operational Data

The TLFFN architecture in Fig. 3 was used for training on available plant data. 100 TLFFNs were trained with 7 input values of accumulated charge (axial SPNDs' readings for an assembly), and 28 output values of relative power corresponding to the assembly's axial power distribution. The input dataset had 44 radial positions as columns per instance of logged data, and a total of 180 instances were used. The output dataset was structured as a 28x7,920 array.

To map the 44x28 power distribution to 133 radial locations without SPNDs, 100 TLFFNs were trained with 44 input values of relative power corresponding to assemblies with SPNDs and 133 output values of relative power corresponding to assemblies without SPNDs. The dataset consisted of 28 axial positions as columns per instance of logged data. The input and output sizes for the entire dataset were 44x7,920 and 133x7,920, respectively.

In all instances of TLFFNs' training, 40% of the data was used as a test to evaluate their performance.

III.E. Convolution Autoencoder Network

A Convolutional Autoencoder Network (CAN) for denoising handwritten digit images **[12]**, was adapted to predict full core power maps from colored indexed images of known power densities. The 14-layer CAN architecture is illustrated in Fig. 4.

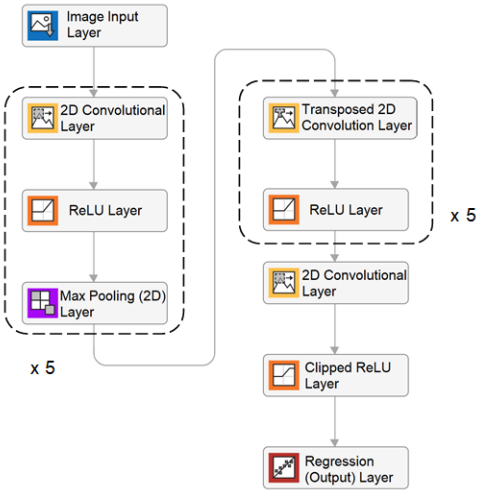

Fig. 4. Convolution Autoencoder Network Architecture.

85 image pairs, corresponding to one of the load schedules, were used to form input and output image data stores with 95% of images for training, and 2.5% for validation and testing, each. 81 image pairs, corresponding to the other load schedule were used as a final test dataset.

III.F. Long Short-Term Memory Networks

Temporal history of charge accumulation data (180 time-steps, at half-hour intervals) was used to train 154 LSTMNs, being half of the total installed SPNDs (308), for sequential charge prediction. For each LSTMN, 90% of the time-series data was standardized and used for training, with 10% for testing. Earlier time steps were used as predictors for the next time step. The LSTMN architecture included a sequence input layer

(accumulated charge), an LSTM layer with 300 hidden units, a fully connected layer, and a regression (output) layer. Testing involved closed-loop forecast for failed detectors, and open-loop forecast for validation against working detectors.

III.G. Core Exit Temperature Distribution Estimation

A simple thermal-hydraulic scheme has been adopted to estimate the core exit temperature. Where the total thermal power generation, $\dot{Q}$, of each assembly has been determined taking into account the losses in the thermal fission process (~2.6%) **[9]**.

From energy conservation considerations for heat transfer from the fuel to the coolant entering the core at a temperature, $T_{\text{in}} = 291.5℃$, with mass flux, $G = 3054\ \text{kg m}^{-2}\ \text{s}^{-1}$ **[9]**, and passing through an effective sub-channel cross-sectional area, A, the coolant's exit temperature, T_{exit}, for each assembly has been calculated using Eq. (1).

$$T_{\text{exit}} = T_{\text{in}} + \frac{\dot{Q}}{289GAc_p} \qquad (1)$$

The second term on the right side of Eq.(1) represents the temperature rise of coolant via heat transfer in 289 (17 x 17 array of) sub-channels, under its' mass flow rate (GA) and specific heat capacity (c_p) at constant pressure, considered to be 6.1236 kJ kg^{-1} $℃^{-1}$; the average of all c_p at temperatures of 291.5, 311.5, 321.5, 326.5, and 330.8℃, corresponding to an average core temperature rise of 39.3℃ **[9]**.

IV. Results and Discussion

IV.A. Regression

From practical considerations, k_{eff} was removed from the predictors due to its invariance ($k_{\text{eff}} \cong 1$). The power level and R-bank limit insertion were co-related, hence $\mathcal{R}$ was removed. The assembly number and spatial coordinates were found to be redundant features, and the assembly number was removed, while the spatial coordinates were kept. Burnup, being a derived feature from power was removed, resulting in a significant reduction in the RMSE. Enrichment and day were incumbently kept because they are potentially significant for subsequent fuel cycles, having different core loading patterns, and account for temporal variation of the power distribution, respectively.

Table I summarizes the effect on RMSE from removing and adding different features on the *Fine Tree Model*, relative to the use of all 9 features (RMSE = 1.5125). The change in RMSE further shows that the model is most sensitive to spatial coordinates and burnup.

Table I. Effect on RMSE for Fine Tree Regression with different combination of Features

S.#	Features	Feature(s) removed	RMSE on Test Data	ΔRMSE (%)
1	8	k_{eff}	1.4856	-1.78
2	7	k_{eff} and Power level	1.4892	-1.54
3	7	k_{eff} and $\mathcal{R}$	1.4991	-0.89
4	6	k_{eff}, $\mathcal{R}$, and Assembly Number	1.4171	-6.31
5	5	k_{eff}, $\mathcal{R}$, x and y	2.2698	+50.1
6	5	k_{eff}, $\mathcal{R}$, Assembly Number, and Burnup	1.2166	-19.6
7	4	k_{eff}, $\mathcal{R}$, x, y and Burnup	1.6078	+6.30

The selected features were used for training and testing other ML models. Overall, the Gaussian Process Regression (GPR) models have performed best in terms of accuracy, but with the lowest rate of prediction. The GPR models' significantly low RMSE can be attributed to their best use case for predicting spatial data **[10]**.

The ANNs performed better than most models as they are well suited for non-linear tasks. Most notably the Wide ANN, which also had the highest predictive speed among all tested models. ANNs have low interpretability, so the raison d'être for RMSE in ANNs cannot be determined with certainty **[10]**.

The Tree models predicted with modest error, taking a significantly brief time for training. Table II lists the performance metrics of representative models on the test dataset.

Table II. Trained Regression Models' Performance for Power Density Prediction

S.#	Model Type	Test		Prediction Rate (s^{-1})
		RMSE	*MAPE*	
1	***Tree***			
	Fine	1.22	1.04	15,428
	Medium	2.82	2.76	44,922
2	***ANN***			
	Wide	0.785	0.740	65,144
	Bi-layered	2.61	2.31	53,497
	Tri-layered	1.73	1.57	47,030
3	***GPR***			
	Squared Exponential	0.289	0.201	9,586
	Matern 5/2	0.240	0.161	7,955
	Exponential	0.270	0.188	9,780

The GUI, based on simulation data, is programmed to predict, and export the core power distribution for any

user-defined day and power from either one of; the GPR Matern 5/2 (Fig. 12), Wide Neural Network, or Fine Tree regression models.

IV.B. Two-Layer Feed-Forward Network

1) Simulation Dataset

The RMSEs of the TLFFNs for the 10% test dataset ranged from 0.0327-0.0535. The TLFFN having the lowest RMSE was tested on each instance of the larger test dataset. The maximum absolute error observed was 0.4061%, corresponding to a MAPE for that instance to be 0.1203%.

The GUI based on simulation data, is programmed to reconstruct the full core power map based on 44 known values of power density (Fig. 13).

2) Plant Operational Data

For the 100 TLFFNs trained to compute axial assembly power profile from charge data, the lowest MSE observed was 0.0077 (MAPE = 5.49%). Fig. 5 shows the plots of MSE of the trained TLFFNs.

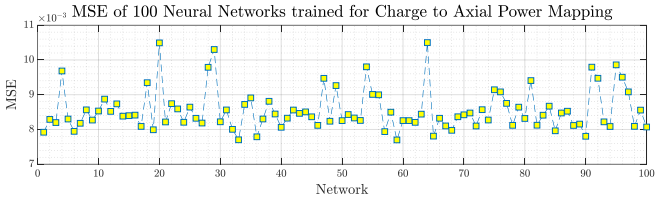

Fig. 5. MSE of 100 Neural Networks trained for 7 Charge to 28 Power Values Mapping.

For 100 TLFFNs trained to compute 133 (non-SPND) from 44 (SPND) power values, the lowest MSE observed was 0.00016 (MAPE = 11.00%). Fig. 6 shows the plots of MSE of the trained TLFFNs.

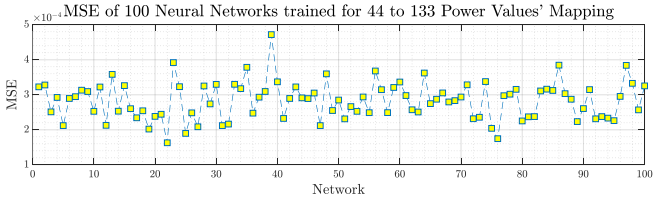

Fig. 6. MSE of 100 Neural Networks trained for 44 to 133 Power Values Mapping.

The random nature of errors in all instances of TLFFNs' training is due to the random nature of how weights and biases of each network are initialized during training **[12]**.

IV.C. Convolution Autoencoder Network

Evaluating the trained CAN for power map reconstruction on the test dataset, the SSIM was computed for each image. Fig. 7, shows the plot of the SSIM, for the test dataset.

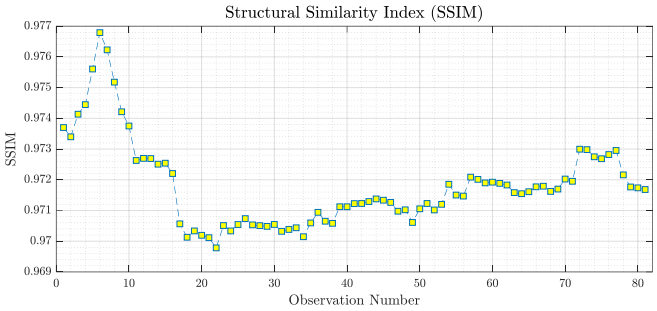

Fig. 7. SSIM from trained CAN on the second simulated load schedule.

Most of the prediction qualities are similar. However, for samples 3-8 and 17-38, the performance either got too good, indicating overfitting, or degraded, indicating underfitting of the CAN, respectively. The phenomena of overfitting and underfitting could have occurred because of similar colored power maps existing in the training dataset. It could also indicate towards the low diversity of the training dataset. An instance of the input, corresponding true output, and predicted image (SSIM=0.9742) from the CAN are shown in Fig. 8.

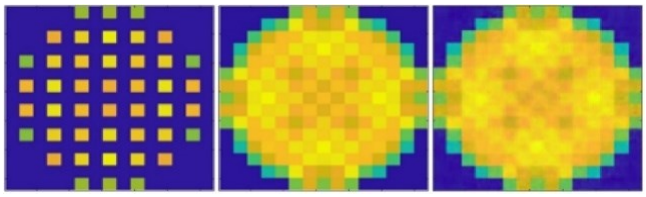

Fig. 8. Sample Input (Left), Actual (Centre), and Predicted (Right) image from the CAN.

IV.D. Long Short-Term Memory Networks

Assessing the trained LSTMNs for charge prediction, using open and closed loop configurations, the prediction and actual charge value plot, and the corresponding error and RMSE were obtained. Fig. 9 and Fig. 10, show these for the 154th LSTMN tested for closed and open loop forecast, respectively.

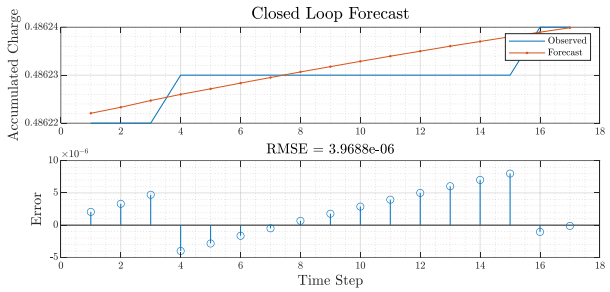

Fig. 9. Closed Loop Forecast and RMSE on predictions for Test Data using the LSTMN for the 154th SPND.

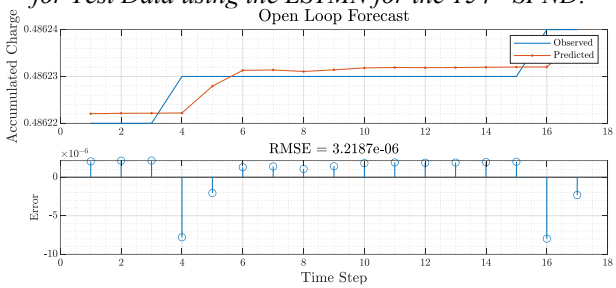

Fig. 10. Open Loop Forecast and RMSE on predictions for Test Data using the LSTMN for the 154th SPND.

Overall, the open loop configuration performed better than the closed loop configuration. This is because the open loop configuration used actual values in prior time steps, in contrast to the closed loop whose predictor for each successive time step is the earlier prediction, which magnifies its' inherent error. The maximum absolute error for both configurations was similar; 0.0016% occurring at time step 16 and 15, respectively.

The GUI (Fig. 11) developed based on operational data reconstructs core power distribution using TLFFNs. LSTMNs used in conjunction, to predict charge for failed SPNDs, allow power map prediction, which is validated using temperature estimation using the scheme in III.G. Errors in temperature for any assembly were seen to be within 1.5% during the simulation of successive failure of SPNDs, up to 180 time-steps.

V. Conclusion and Recommendations

This study explored machine learning techniques for in-core power mapping of an HPR1000 using reactor simulations and available operational data. For the simulation dataset, using feature selection, the original parameters have been reduced to 5, for power density prediction. Based on these predictors, the Wide ANN's performance was excellent in terms of accuracy and speed of prediction.

TLFFNs performed well for core power map reconstruction. The combined use of TLFFNs and LSTMNs proved to be suitable for extending plant operation during multiple detector failures, for up to 50% of all SPNDs' failure. Temperature prediction based on power predictions enabled ascertaining the error during prediction.

The current models trained with limited data, and the combined use of multiple networks, increases error. This can be overcome by diversifying data, specifically covering different known states of the core. Future work should also focus on hyperparameter optimization and investigating the performance of other ANN architectures. Additionally, feature engineering techniques can be explored to improve charge-to-power mapping, such as deriving instantaneous charge or current for each time step.

Use of high-resolution images and finer convolution filters with the support of Graphical Processing Units could improve the CAN's performance.

Finally, a more detailed and rigorous Thermal-Hydraulic Analysis, incorporating available correlations **[15]** and validating against actual temperature measurements for known states of the HPR1000 reactor, is necessary to further validate the proposed scheme for meeting the LCO reliably.

By addressing these recommendations and considering subsequent fuel cycles, including the effect of assembly enrichment, the current approach can be further validated, refined, and fortified.

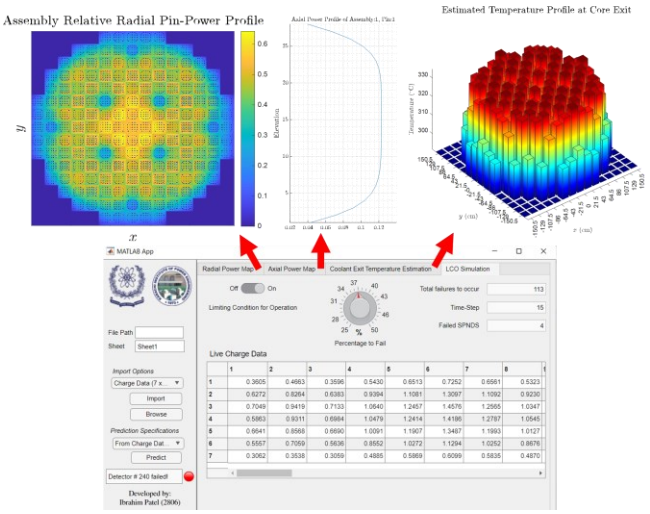

Fig. 11. GUI Functionality Overview.

Acknowledgment

The Pakistan Atomic Energy Commission is thanked for facilitating this research at their prestigious training center.

Appendix

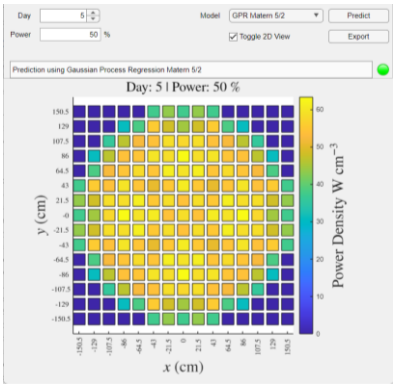

Fig. 12. Power Density Prediction using the GPR Matern 5/2 Regression Model.

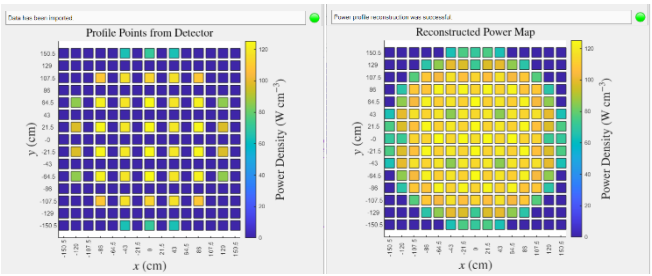

Fig. 13. Power Density Profile Reconstruction from 44 locations (Left) to Full Core Map (Right).

References

1. International Atomic Energy Agency: Artificial Intelligence for Accelerating Nuclear Applications, Science and Technology. Artif. Intell. Accel. Nucl. Appl. Sci. Technol. 1–98 (2022).

2. Ma, Z., Bao, H., Zhang, S., Xian, M., Mack, A.: Exploring Advanced Computational Tools and Techniques with Artificial Intelligence and Machine Learning in Operating Nuclear Plants. United States Nuclear Regulatory Commission (2022).

3. Li, W., Ding, P., Xia, W., Chen, S., Yu, F., Duan, C., Cui, D., Chen, C.: Artificial Neural Network Reconstructs Core Power Distribution. Nucl. Eng. Technol. (2021). https://doi.org/10.1016/j.net.2021.08.015

4. Li, W., Ding, P., Duan, C., Qiu, R.X., Lin, J., Shi, X.: Comparison of Spatial Interpolation Approaches for In-Core Power Distribution Reconstruction. Nucl. Eng. Des. 337, 66–73 (2018). https://doi.org/10.1016/J.NUCENGDES.2018.06.016

5. Saeed, A., Rashid, A.: Development of Core Monitoring System for a Nuclear Power Plant using Artificial Neural Network Technique. Ann. Nucl. Energy. 144, (2020). https://doi.org/10.1016/j.anucene.2020.107513

6. Pirouzmand, A., Dehdashti, M.K.: Estimation of Relative Power Distribution and Power Peaking Factor in a VVER-1000 Reactor Core using Artificial Neural Networks. Prog. Nucl. Energy. 85, 17–27 (2015). https://doi.org/10.1016/j.pnucene.2015.06.001

7. China National Nuclear Corporation: Two units of the first overseas project of HPR1000 officially delivered, https://en.cnnc.com.cn/2023-02/02/c_851939.htm

8. Peng, X., Li, Q., Wang, K.: Fault Detection and Isolation for Self Powered Neutron Detectors based on Principal Component Analysis. Ann. Nucl. Energy. 85, 213–219 (2015). https://doi.org/10.1016/j.anucene.2015.05.016

9. Nuclear Power Institute of China: Hualong One Final Safety Analysis Report.

10. The MathWorks Inc.: Machine Learning with MATLAB. The MathWorks, Inc. (2022).

11. Hagan, M.T., Demuth, H.B., Beale, M.H., De Jesús, O.: Neural Network Design. Hagan and Demuth (2014).

12. The MathWorks Inc.: Deep Learning Toolbox™ User's Guide R2022b, (2022).

13. Makai, M., Végh, J.: Lecture Notes in Energy 58 Reactor Core Monitoring Background, Theory and Practical Applications. Springer (2017).

14. Nuclear Power Institute of China: Hualong One Detail Design I&C System Manual RII In-Core Instrumentation System.

15. Masterson, R.E.: Nuclear Reactor Thermal Hydraulics an Introduction to Nuclear Heat Transfer and Fluid Flow. CRC Press (2019).